Polymer 49 (2008) 5705–5713

Contents lists available at ScienceDirect

Polymer

journal homepage: www.elsevier.com/locate/polymer

Initial structure development in the CO_2 laser-heated drawing of poly(trimethylene terephthalate) fiber

KyoungHou Kim [a], YoungAh Kang [b], Takahisa Murata [b], Soichiro Ikehata [b], Yutaka Ohkoshi [b,*], Yasuo Gotoh [b], Masanobu Nagura [b], Mitsuharu Koide [c], Hiroshi Urakawa [c], Masaru Kotera [d]

[a] Collaborative Innovation Center for Nanotech FIBER (nanoFIC), Shinshu University, Ueda Nagano 386-8567, Japan
[b] Faculty of Textile Science and Technology, Shinshu University, 3-15-1 Tokida Ueda Nagano, Japan
[c] Faculty of Engineering and Design, Kyoto Institute of Technology, Goshokaidoucho, Matsugasaki, Sakyo-ku, Kyoto 606-8585, Japan
[d] Department of Chemical Science and Engineering, Faculty of Engineering, Kobe University, Rokko, Nada, Kobe 657-8501, Japan

ARTICLE INFO

Article history:
Received 21 May 2008
Received in revised form 9 October 2008
Accepted 12 October 2008
Available online 1 November 2008

Keywords:
Poly(trimethylene terephthalate)
Initial fiber structure development
On-line measurements

ABSTRACT

Because rapid and uniform laser heating can fix the neck-drawing point in continuous drawing of PTT fiber, we have successfully analyzed the fiber structure development in the continuous drawing process by in-situ measurement with a time resolution of less than 1 ms. In this study, we investigated fiber structure development for PTT around the neck point controlled with a CO_2 laser-heated apparatus during continuous drawing, through on-line measurements of WAXD, SAXS, and fiber temperature. Fiber temperature attained by laser radiation initiated a rise around −3 mm in relation to the neck point at 0 mm, and increased to about 90 °C, which is past the 45 °C T_g for PTT. The instantaneous increase in fiber temperature continued with a vertical ascent, with plastic deformation around the neck point. The crystalline diffraction pattern was revealed initially at the elapsed time of 0.415 ms immediately after necking, and remained fairly constant with elapsed time. The ultimate crystalline diffraction pattern for a completely drawn fiber showed little difference from that at the initial stage. In PET a two-dimensionally ordered structure in the form of a mesophase was detected immediately after the necking, whereas in PTT the phenomenon was not observed. With elapsed time, the d spacing of (002) plane decreased gradually due to transformation of the initial *all-trans* conformation into *trans-gauche-gauche-trans* conformation, and ultimately the PTT molecular chain could favorably adopt the *trans-gauche-gauche-trans* conformation. SAXS pattern immediately after the necking revealed an X-shape; the scattering intensity concentrated on meridian directions due to individual crystal development, and at 2 ms two-pointed scattering started to appear. Past 8 ms, the typical two-pointed scattering pattern was prominent and its intensity increased with elapsed time. Long period decreased with increasing elapsed time, but the crystallite size of meridian (002) plane hardly changed. The decrease in long period might be caused by chain relaxation in the amorphous region.

1. Introduction

Although the polymerization of poly(trimethylene terephthalate) (PTT) was first reported by Whinfield and Dickson of Caligo Printing Ink Co. in 1941, the commercial production of PTT was not realized until the mid 1990s, when the manufacturing cost of 1,3-propanediol dropped drastically [1]. Unlike PET and poly (butylene terephthalate) (PBT), which have even numbers of methylene units, PTT has excellent properties, such as elastic recovery and dyeability, owing to its odd number of methylene units, and its mechanical performances exists roughly between those of PET and PBT.

The crystal structure of PTT was determined by some researchers for samples prepared under various conditions [2–5]. Only one crystalline form has been reported, and the unit cell was found to be triclinic. The reported unit cell parameters for a melt-crystallized PTT sample are $a = 0.464$ nm, $b = 0.627$ nm, $c = 1.864$ nm, $\alpha = 98.4°$, $\beta = 93.0°$, and $\gamma = 111.1°$, with crystalline density being 1.40 g/cm^3 and amorphous density being 1.299 g/cm^3 [4,6]. The flexible part consists of a three-methylene group sequence with an energetically favored *trans-gauche-gauche-trans* conformation. Semicrystalline PTT samples have been subjected to a detailed thermal analysis [7], where glass transition and typical onset temperatures of melting endotherm were reported to be 58 and 216 °C, respectively. For 100% crystalline PTT, the heat of fusion is estimated to be 30 ± 2 kJ/mol.

* Corresponding author.
E-mail address: yokoshi@shinshu-u.ac.jp (Y. Ohkoshi).

0032-3861/$ – see front matter © 2008 Elsevier Ltd. All rights reserved.
doi:10.1016/j.polymer.2008.10.022

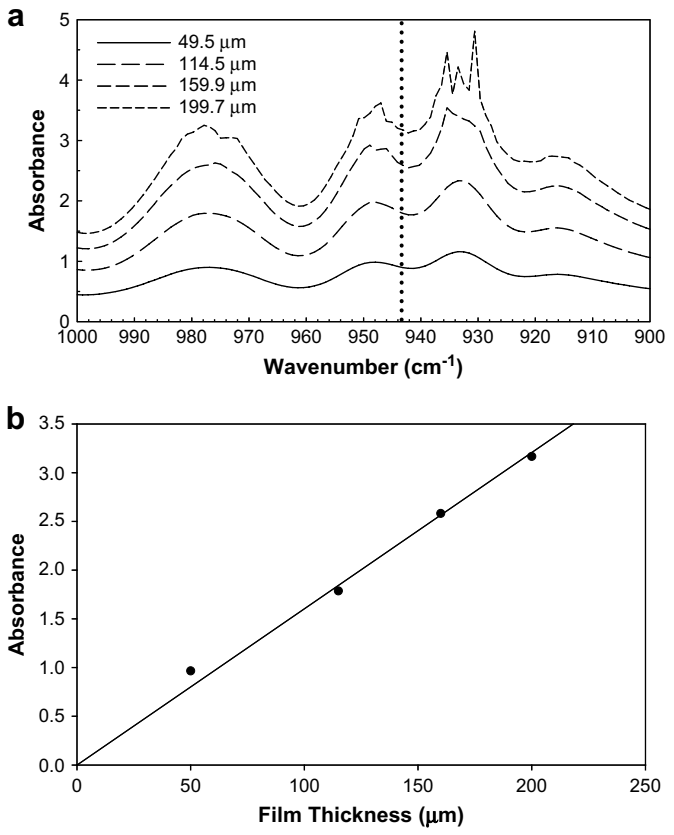

Fig. 1. (a) FT-IR spectra of PTT films with various thicknesses, (b) IR absorbance at 943 cm^{-1} as a function of film thickness.

Several studies have been conducted for the on-line characterization of structure development for synthetic fibers during drawing using simultaneous synchrotron radiation as well as laboratory x-ray generators for WAXD and SAXS [9–11]. Schultz et al. [8] reported that unit cell dimensions, crystallinity, and orientation were dependent on stretching temperature and strain. Moreover, they suggested a model of lateral growth of crystallite with extended chains as nucleation sites for PTT. The drawing behaviors of nylon 66 and PET have been studied by Hsiao et al. [12] and Ohkoshi et al. [13,14], respectively.

Neck drawing is particularly important, because structure and properties of synthetic fibers are mainly determined by this very complex process, in which fiber diameter changes steeply, molecular chains align to fiber axis, and fiber structure is developed through orientation-induced crystallization within a few milliseconds. For the neck drawing process, our research group has accomplished a quantitative analysis on the fiber structure development mechanism by direct measurement in the vicinity of the neck point. We have reported on the on-line measurements for drawing behavior [13,14], fiber temperature changes, and WAXD/SAXS, in which the data were obtained as functions of time elapsed after necking. The elapsed time, which is calculated from the distance between the measurement point and the neck-drawing point, has high accuracy because the neck-drawing point could be fixed within confined region by rapid and uniform heating of running fiber with irradiation with a CO_2 laser. We have succeeded in the on-line measurement by this procedure [14], where the fiber structure development could be analyzed quantitatively within a time resolution of 1 ms for X-ray diffraction measurement and 0.47 ms for fiber temperature profile for the PET running fiber.

The initial structure development for PET fiber has been studied extensively, and various researchers, including our group, have achieved valuable results. However, to our knowledge, structure development of PTT fibers during drawing has not been addressed. Therefore, in the present study, we investigated fiber structure development around the neck point controlled with the CO_2 laser-heated apparatus during continuous drawing, through the on-line measurements of WAXD, SAXS, fiber temperature, and drawing stress with a time resolution of 0.43 ms.

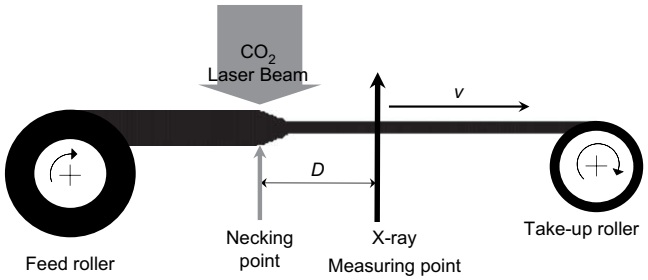

Fig. 2. Schematic diagram of the in-situ measurement system. Elapsed time after necking can be calculated from the running speed v of fiber and the distance D between the neck point and the measurement point.

2. Experimental

2.1. CO_2 laser absorption coefficient

The absorption coefficient of CO_2 laser for PTT was characterized by means of an infrared spectrometer. The wavelength used for the CO_2 laser is 10.6 μm, corresponding to 943 cm^{-1}. The infrared absorption at this point was plotted against PTT film thickness, and the absorption coefficient was obtained by extrapolation. The obtained absorption coefficient for PTT was found to be 3.42×10^4 m^{-1}, which corresponds to approximately triple that of PET. Fig. 1(a) and (b) shows the infrared spectrum and absorption coefficient for PTT film, respectively.

2.2. Fundamentals of on-line measurement

Fig. 2 shows a schematic diagram of the on-line measurement system used in this study. Details of the on-line system can be found in our previous papers [13,14]. The running fiber was heated through irradiation by a CO_2 laser beam generated by a PIN-20S laser source manufactured by Onizca Glass Co. Ltd. The laser source has a rated power of 20 ± 1 W, and a laser beam diameter of 5 mm. The fiber was

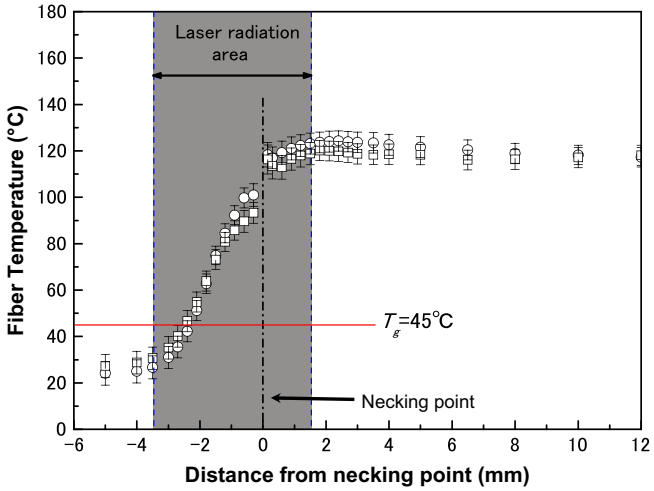

Fig. 3. Fiber temperature profiles along the before and after necking with distance from the laser axis for PTT fiber. Fiber temperature was measured twice to get accuracy.

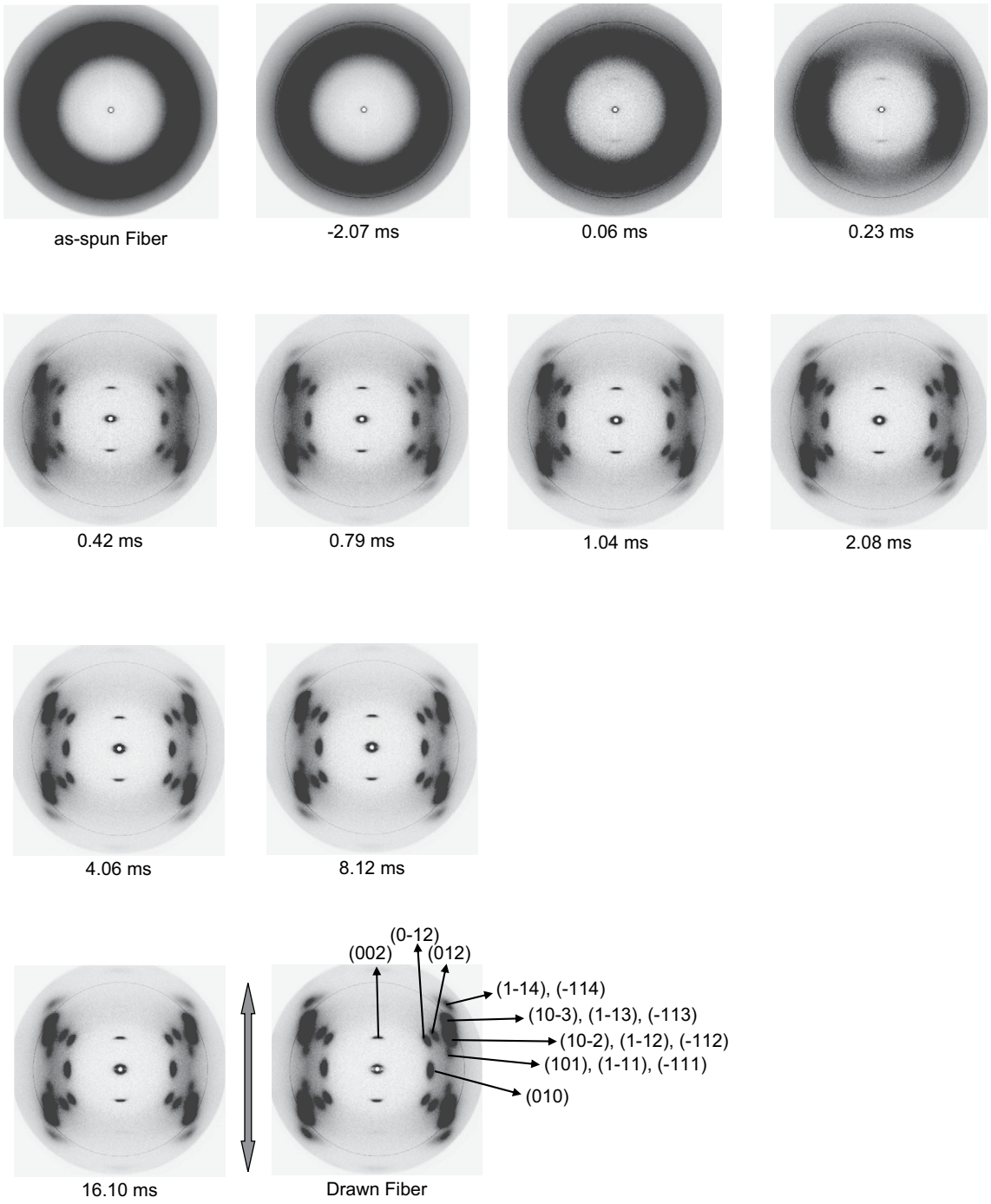

Fig. 4. WAXD images of PTT fibers obtained at various elapsed times during the laser-heated neck drawing. The reflection indices are marked in the pattern of the drawn fiber, and the arrow indicates the stretching direction.

drawn by means of a speed differential between the feed and take-up rollers. Control of the neck-drawing point within 1 mm by laser irradiation maintained a well-stable and well-steady state for the neck drawing. X-ray diffraction images were recorded, and fiber temperature was measured as a function of elapsed time t, which was calculated from the distance from the neck-drawing point x divided by fiber running speed v. The distance x was controlled by shifting neck deformation point with a traveling mirror unit.

2.3. Materials and drawing conditions

PTT pellets having an intrinsic viscosity 0.92 dl/g were spun while a mass flow rate of 5.0 g/min was maintained, along with a take-up speed of 120 m/min. An as-spun PTT monofilament of 200 μm in diameter was drawn up to a draw ratio 4.2 with a feed speed of 14 m/min and a take-up speed of 58.8 m/mim, where drawing stress was 28 MPa.

2.4. Fiber temperature measurement

Fiber temperature was measured with an infrared thermometer manufactured by Japan Sensor Co. Ltd. An HgCdTe detector was used for the thermometer, and response time was 10 ms. The thermometer was equipped with an interference filter of wavelength 5.78 μm, which corresponds to the stretch vibration of the carbonyl group in PTT. Further details for on-line

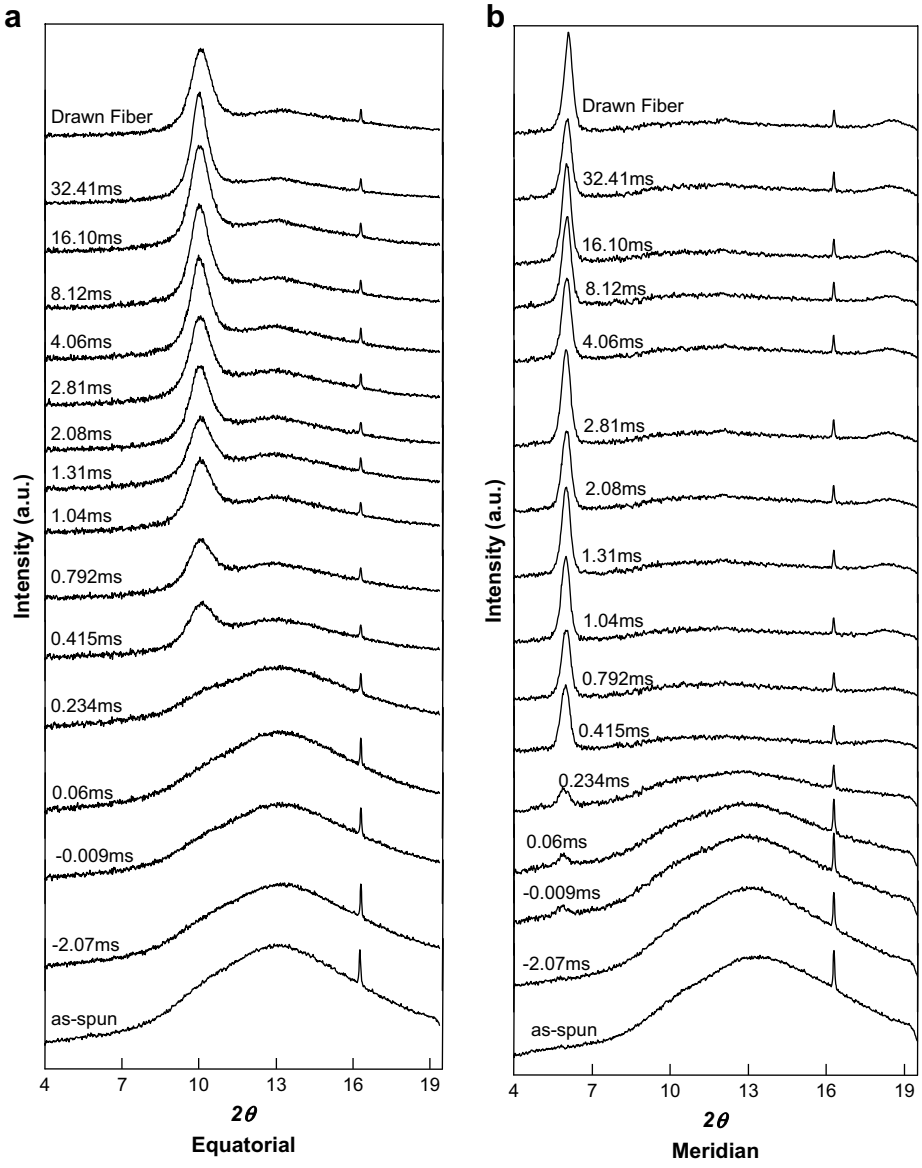

Fig. 5. X-ray intensity profiles for PTT fibers: (a) equatorial direction (b) meridian direction. Elapsed times are noted in the inset.

fiber temperature measurement can be found in our previous reports [15–17].

2.5. X-ray characterization

Synchrotron radiation of BL40B2 in SPring-8 was used for this study. The applied wavelength for WAXD was 0.1 and that for SAXS was 0.15 nm, and diameter was about 210 μm. The X-ray diffraction images were taken by 3000 × 3000 pixel imaging plates attached to vacuum chambers of 400 mm and 2000 mm lengths for WAXD and SAXS, respectively. The sample-to-detector distance was calibrated using lead stearate (StPb) for WAXD and collagen for SAXS. The exposure time was 4 min for WAXD and 30 min for SAXS. The neck deformation point was located by a transmitted x-ray intensity

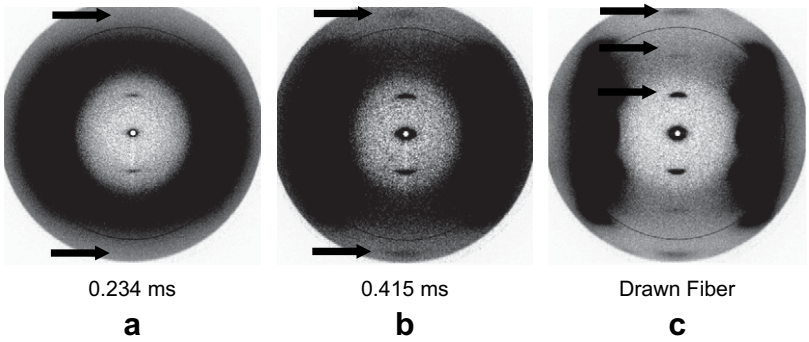

Fig. 6. WAXD images of increased darkness in order to intensify the meridian streak.

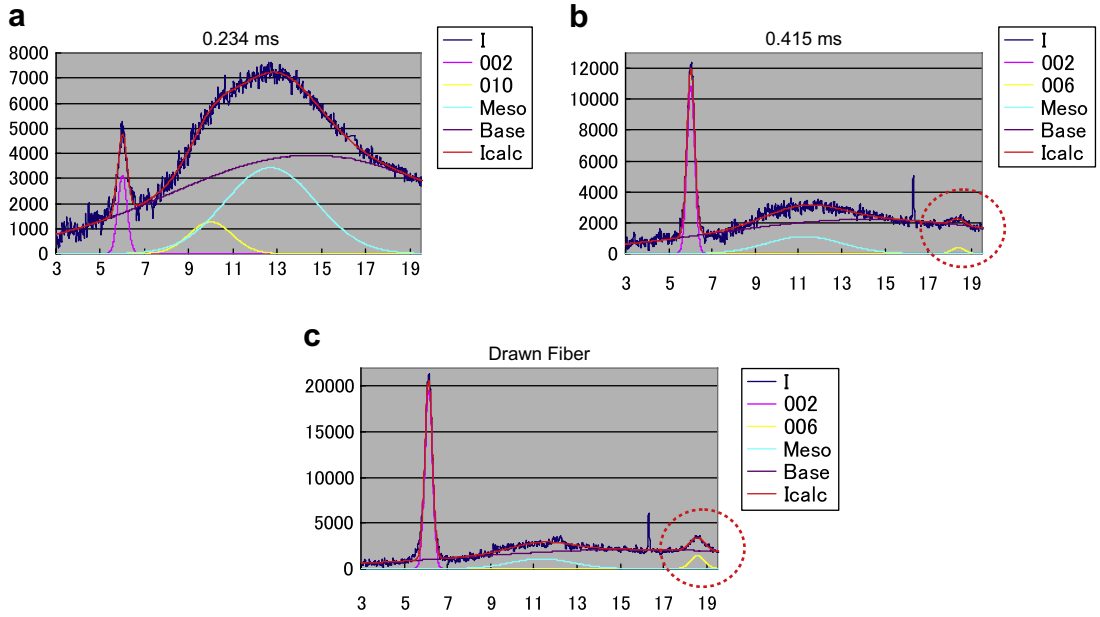

Fig. 7. Meridian intensity profiles including peak separation result.

profile through an ion chamber. The intensity profile containing diffraction by polyimide film mounted on the vacuum chamber could be used as a reference profile by subtracting a blank image. Additional details for the on-line X-ray diffraction characterization can be found in our previous reports [13,14].

The position θ_0 and the half width σ were determined by fitting with a Gauss function (Eq. (1)). The beam divergence effect on σ was corrected with the width of intensity profiles of StPb. The d spacing d and structure size D were calculated by Bragg's equation (Eq. (2)) and Scherer's equation (Eq. (3)), where the constant k in Eq. (3) is 0.918. The crystal orientation factor f was obtained from the azimuthal intensity profiles of equatorial (010) and meridian (002) planes fitted by Pearson VII function (Eq. (4)), with an assumption that τ is similar to measured half width of these planes. The crystal orientation f was calculated with Eq. (5) by integrating the fitted profiles.

$$I(\varphi) = I_0 \exp\left\{ -4\ln 2\left(\frac{\theta-\theta_0}{\sigma}\right)^2 \right\} \tag{1}$$

$$2d \sin\theta_0 = \lambda \tag{2}$$

$$D = \frac{k\lambda}{\sigma \cos\theta_0} \tag{3}$$

$$I(\beta) = -\frac{I_0}{\left\{1+4\left(\frac{\beta-\beta_0}{\tau}\right)^2\left(2^{\frac{1}{2.5}}-1\right)\right\}^{2.5}} \tag{4}$$

$$f = \frac{3\langle\cos^2\beta\rangle - 1}{2}, \langle\cos^2\beta\rangle = \frac{\int_0^{\pi/2} I(\beta)\cos^2\beta\sin\beta\,d\beta}{\int_0^{\pi/2} I(\beta)\sin\beta\,d\beta} \tag{5}$$

Correlation function ($\gamma(r)$) analysis was adopted to quantitatively analyze the lamellar structure. For this analysis, a projection operation was first applied to obtain the integrated intensity on the meridian directions ($I_1(q_3)$) by Eq. (6), where, $q(=4\pi\sin\theta/\lambda)$ is the scattering vector. The subscript 3 represents the meridian direction, and the subscript 12 represents the equatorial direction. After obtaining $I_1(q_3)$, a 1D Fourier transition was then applied in order to obtain the correlation function of Eq. (7). Using the method [18] proposed by Strobl and Schneider and assuming a lamellar two-phase morphology, the long period L and the lamellar and amorphous layer thicknesses can be evaluated.

$$I_1(q_3) = \int_0^\infty I(q_{12},q_3)q_{12}\,dq_{12} \tag{6}$$

$$\gamma(x) = \frac{\int_0^\infty I_1(q_3)\cos(q_3x)dq_3}{\int_0^\infty I_1(q_3)dq_3} \tag{7}$$

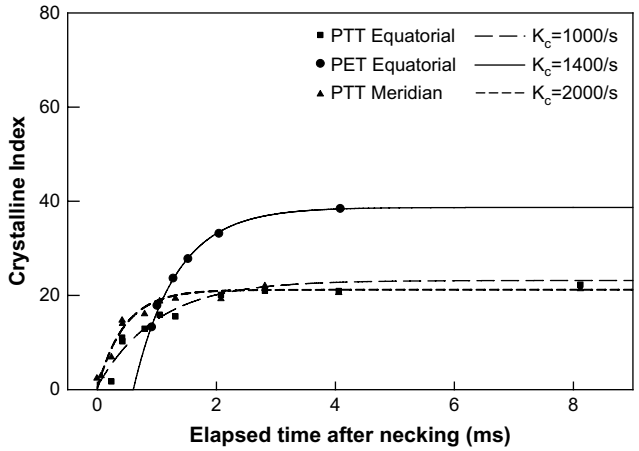

Fig. 8. Changes of the crystallinity indices for PTT fibers in the equatorial and meridional directions, and for PET fiber in the equatorial direction with elapsed time. The crystallization rates (Kc) were shown in legend.

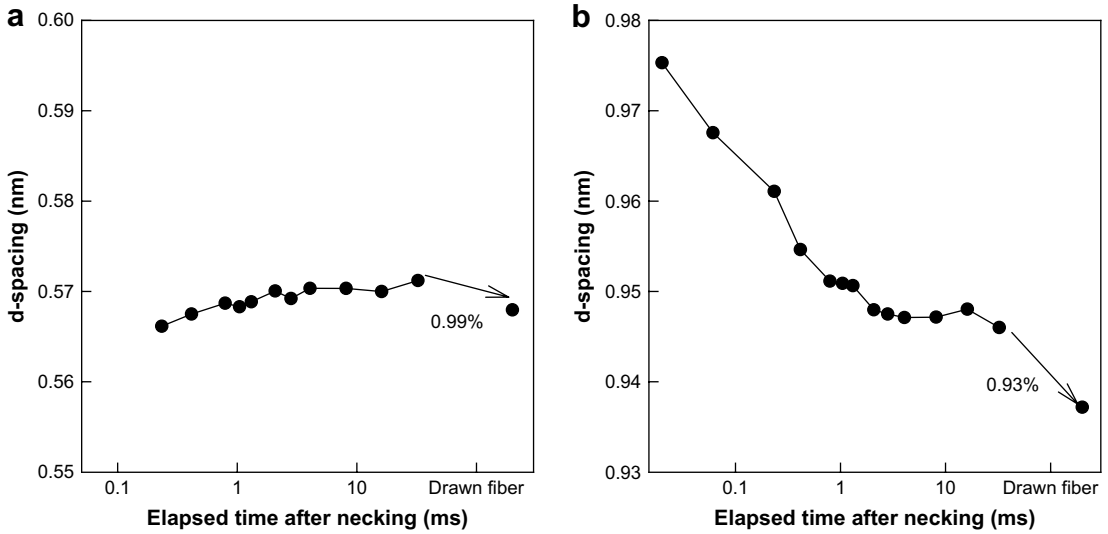

Fig. 9. Interplanar spacing calculated for (010) (a) and (002) (b) diffractions for PTT fibers.

3. Results and discussion

3.1. Temperature profile

Fig. 3 shows fiber temperature profile with distance from the neck point during the laser-heated drawing of PTT fiber, where zero on the horizontal axis indicates the neck deformation point, and the region between two dotted lines denotes the laser radiation area. The fiber temperature of PTT fiber increased steeply immediately upon entering the laser radiation region. Due to the laser radiation, the fiber temperature initiated a rise about −3 mm away from the neck point 0 mm and increased to about 90 °C, which is greater than the T_g 45 °C for PTT. The instantaneous increase in fiber temperature continued as a vertical ascent with plastic deformation around the neck point. Then, the fiber temperature gently increased up to 120 °C as a result of an exothermic reaction by crystallization, and finally reached a saturation level after 3 mm.

3.2. WAXD analysis

Fig. 4 shows WAXD images taken at various elapsed times during the laser-heated drawing for PTT fiber. Fig. 5 shows the equatorial and meridian intensity profiles with elapsed time. The initially observed amorphous halo started a concentration in the equatorial plane immediately after the neck point, and simultaneously the meridian streak emerged. The equatorial (010) diffraction revealed at 0.415 ms indicates the formation of fiber structure by orientation-induced crystallization. The results show that the crystallization for PTT occurs at about one-tenth the time as compared with that for PET reported in our previous report [13]. Thus, little appearance of mesophase structure in the fiber structure development for PTT was observed, unlike the case of PET, which formed the mesophase structure during orientation-induced crystallization after assuming a two-dimensionally ordered structure. The intensity of crystalline diffraction increased with elapsed time by about 1 ms, and thereafter the intensity level was

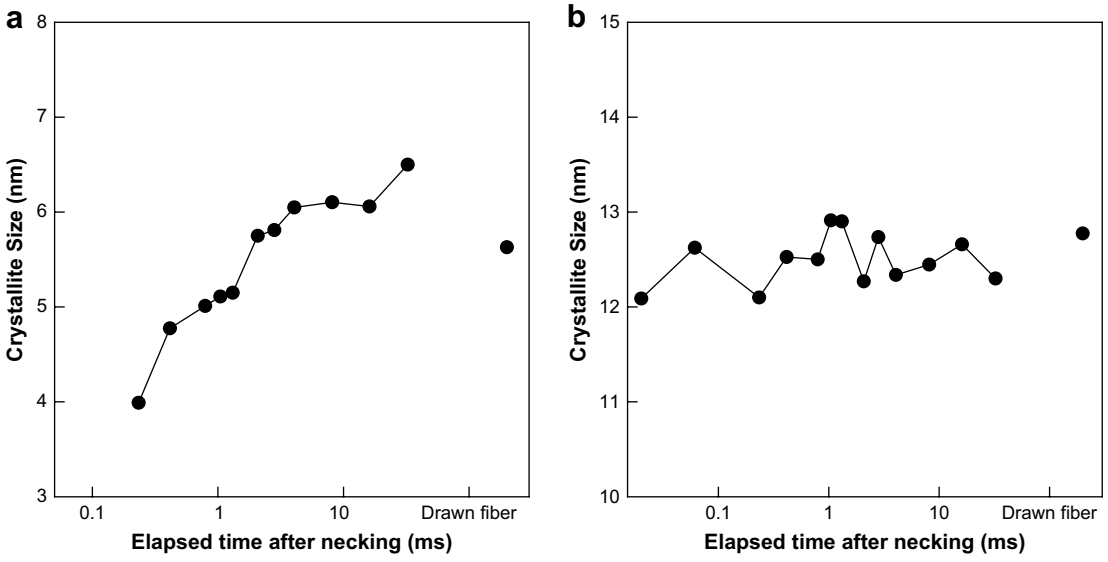

Fig. 10. Crystallite sizes calculated for (010) (a) and (002) (b) diffractions for PTT fibers.

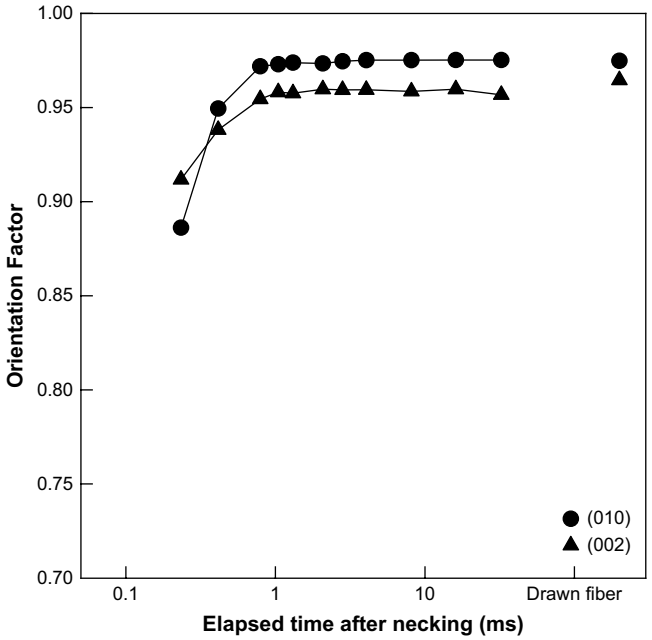

Fig. 11. Crystalorientation factor calculated from (010) (a) and (002) (b) diffractions for PTT fibers.

equivalent to that of the drawn fiber. The fiber structure development for PTT seemed to be completed within 1 ms after the neck deformation. The meridian (002) diffraction was observed earlier than the equatorial diffraction, and occurred together with the initiation of neck deformation. Hence, the molecular chain might be initially oriented along the fiber axis, and then the crystalline order in equatorial might be developed. Therefore, the structural development process for PTT could be regarded as a shish–kebab structure, in which a shish structure might be formed initially and then the crystalline structure might be grown up laterally. In particular, in the meridian profile (see Fig. 5(b)), the (006) diffraction around $2\theta = 18.5^\circ$ was found simultaneously with the initiation of the neck deformation, and its intensity increased with elapsed time. This might be due to an increase of crystalline order in the meridian direction. In addition, a very weak streak regarded as that by (004) diffraction could be observed at 2θ between the (002) and (006) diffractions. Fig. 6 shows WAXD images under increased darkness so as to exaggerate the meridian streak, and three streaks of (002), (004), and (006) diffractions in the respective first, second, and third layer lines are clearly revealed in the drawn fiber. Fig. 7 shows the meridian intensity profile and its peak-fitted result to quantitatively manifest the meridian diffractions. The (006) diffraction increased with elapsed time, whereas the (004) diffraction could not be separated from amorphous scattering. Schultz et al. reported that the meridon streak implies a microfibrillar entity and the shish may be the reciprocal image of a long thin fibril [8]. Accordingly, the fiber structure development process for PTT seems to begin with the shish structure, which is followed by the kebab structure of lamella. As a matter of fact, it

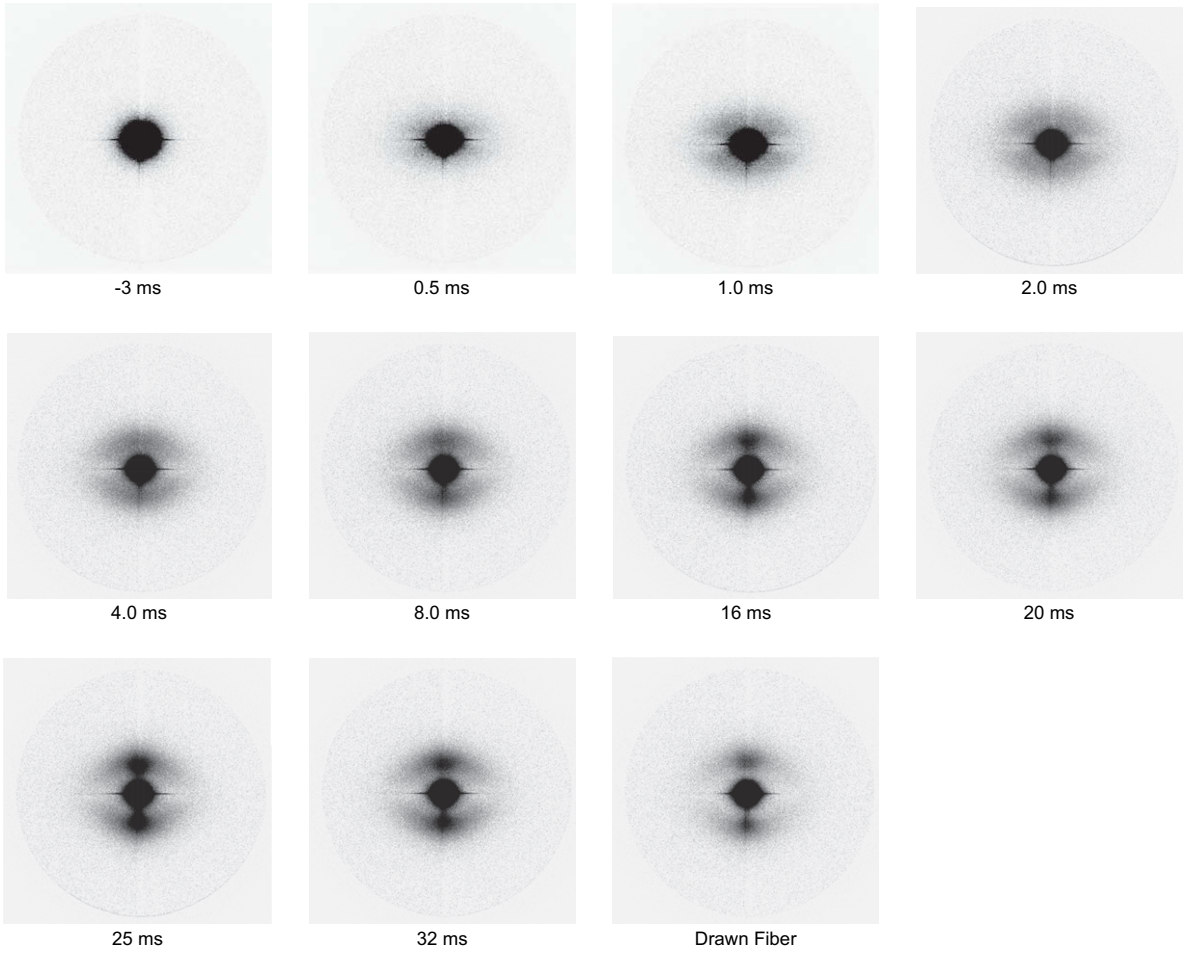

Fig. 12. SAXS images of PTT fibers obtained at various elapsed times during the laser-heated neck drawing.

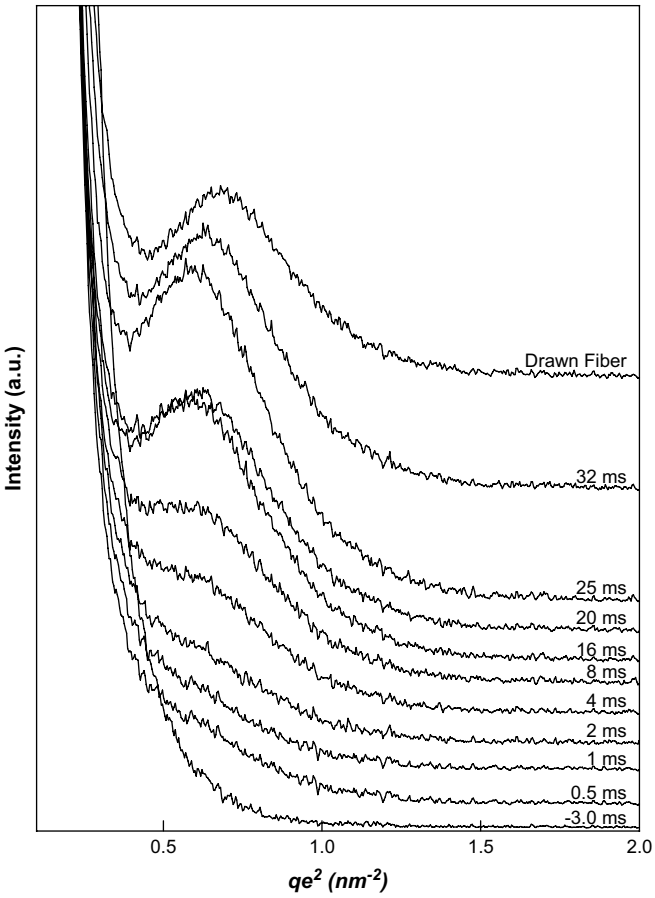

Fig. 13. SAXS intensity profiles for PTT fibers: elapsed times are noted in the inset.

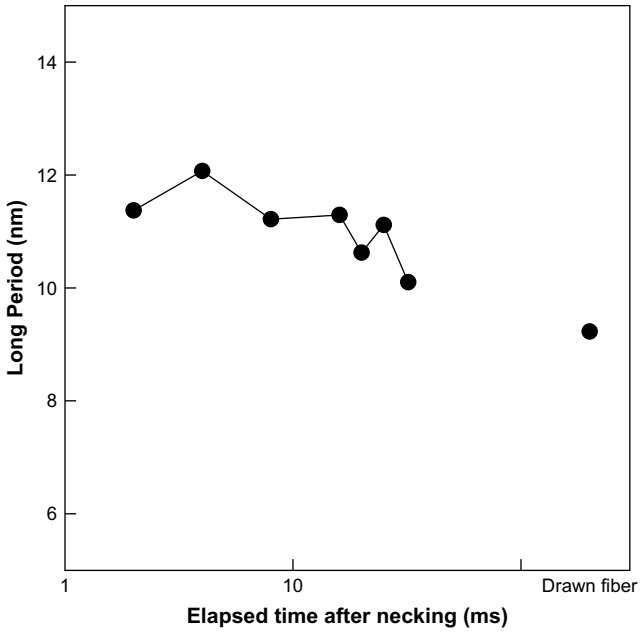

Fig. 14. Long period obtained from SAXS intensity profiles for PTT fibers.

may be apprehended that the (004) and (006) diffractions was observed due to fluctuation of the chain axis. There are some reflections of almost identical d spacing with the (006) diffraction, such as (−114) reflection, but the diffractions are least likely to be revealed because of being away from the meridian. Furthermore, the (004) and (006) diffractions became more obvious after the necking, where the integrity of crystal structure might increase due to relaxation effects such as thermal shrinkage, and accordingly the emergence of (004) and (006) diffractions may be ascribed to total effect by helix structure and tilting of crystal for PTT. Detailed discussion on crystallization rate and crystallite size continues in the following section.

3.3. Crystallization rate

The crystalline diffraction peaks in equatorial and meridian was separated by peak-fitting, the crystallinity indices in the equatorial and meridian directions were calculated from areas of their separated peaks, and the crystallization rate was calculated by the Avrami equation (Eq. (8)).

$$\chi = \{1 - \exp(-Kt)\}\chi_{DSC} \tag{8}$$

Fig. 8 shows the crystallinity indices in the equatorial (square) and meridian (triangle) directions for PTT with elapsed time, and for comparison the crystallinity index for PET. The regression lines were obtained by Eq. (8), and the calculated crystallization rates K_c were presented. The crystallinity index increased steeply by approximately 1 ms and then leveled off. The crystallization rates K_c in the equatorial and meridian directions were 1000 and 2000 s^{-1}, respectively, and subsequently the crystallization rate in the meridian directions was twice as fast as in the equatorial direction. Thus, in the fiber structure development of PTT, the shish structure may be formed initially after the neck deformation and then the kebab structure may be developed. Alternatively, the averaged crystallization rate for PTT in the equatorial and meridian directions is almost equivalent to that of PET. The crystallization induction time is close to zero for PTT, but falls within the range of 0.6–1 ms for PET [14]. This constitutes direct evidence that the initiation of crystalline formation by orientation-induced crystallization is much earlier than that for PET. Little mesomorphologic structure such as the two-dimensionally ordered structure observed in the fiber structure development of PET could be revealed, due to the crystal forming immediately after the neck deformation. Although the crystal growth should affect the integrated intensity both in the equatorial and meridian reflections, in this study, especially, it would be discussed that the meridian diffraction was developed firstly prior to appearance of the equatorial diffraction and the meridian diffraction intensity increased with elapsed time.

Fig. 9 shows d spacing changes of the equatorial (010) and meridian (002) planes with elapsed time. The (010) d spacing hardly changed with elapsed time, but the (002) d spacing decreased gradually. Flattened change for the (010) d spacing may reflect little structural relaxation after the completion of drawing. As has been reported by Schultz et al. [8], the drawing of PTT POY changed the *c* length of unit cell parameter from 18.6 to 23.6 Å, which might reflect a conformational change from *trans-gauche-gauche-trans* into *all-trans*. The conformational change during the drawing was observed in our study. Earlier than 1 ms, the (002) d-spacing shrank in an intermediate level between *trans-gauche-gauche-trans* and *all-trans* conformations. Then, with further elapsed time, a stable structure close to *trans-gauche-gauche-trans* conformation was developed and ultimately, after drawing, transformed into the *trans-gauche-gauche-trans* structure.

Fig. 10 plots the crystallite size for the equatorial (010) and the meridian (002) planes according to Scherer's equation (Eq. (3)) with elapsed time. The crystallite size for the (010) plane increased with elapsed time, but little change is seen for the (002) plane. Thus, with elapsed time, the longitudinal growth of crystallite after the neck deformation was not observed, but the transverse increase was developed. The longitudinal structure development, which

may indicate the growth of shish, seemed to be completed within 1 ms, whereas the crystallite size for the (010) plane, which may denote the growth of kebab structure, increased gradually after the neck deformation and reached the equivalent size of the drawn fiber at later than 2 ms. As a result, in the fiber structure development for PTT, the (002) reflection was developed preferentially after the neck deformation and underwent little change in crystallite size. On the other hand, the crystallite size for (010) plane increased up to 2 ms after the neck deformation.

Fig. 11 shows the crystalline orientation factors for the equatorial (010) and meridian (002) planes with elapsed time. The crystalline orientation reached a maximum orientation level within 1 ms, and then hardly changed. The crystalline orientation factors after the neck deformation are very high close to 1, indicating that the crystalline orientation attained a good level.

3.4. Ultra small-angle x-ray analyses

Fig. 12 shows Ultra SAXS images obtained at various elapsed times before and after the neck deformation. Fig. 13 shows the intensity profiles with elapsed time. The scattering pattern immediately after necking revealed an X-shape; the scattering intensity concentrated on meridian directions due to an individual crystal development, and at 2 ms two-pointed scattering started to appear. Past 8 ms, the typical two-pointed scattering pattern is obvious, and its intensity increased with elapsed time.

Fig. 14 shows long period calculated from the SAXS intensity profiles. The long period decreased with increasing elapsed time. However, in the WAXD results shown previously, the crystallite size of the meridian (002) plane hardly changed with elapsed time. The decrease of long period with elapsed time could be caused by chain relaxation in the amorphous region during drawing.

4. Conclusion

In this study, we investigated fiber structure development for PTT around the neck point controlled with a CO_2 laser-heated apparatus during continuous drawing, through on-line measurements of WAXD, SAXS, and fiber temperature. The crystalline diffraction pattern was revealed initially at the elapsed time of 0.415 ms immediately after necking, and remained fairly constant with elapsed time. The crystallization rate for PTT averaged in the equatorial and meridian directions was equivalent to that for PET, and the crystallization induction time for PTT was close to 0 ms while in the range of 0.6 ~ 1 ms for PET. With elapsed time, the d spacing of (002) plane decreased gradually due to transformation of the initial *all-trans* conformation into *trans-gauche-gauche-trans* conformation, and ultimately the PTT molecular chain could favorably adopt the *trans-gauche-gauche-trans* conformation. SAXS pattern immediately after the necking revealed an X-shape; the scattering intensity concentrated on meridian directions due to individual crystal development, and at 2 ms two-pointed scattering started to appear.

Acknowledgements

The synchrotron radiation experiments were performed at the BL40B2 in the SPring-8 with the approval of Japan Synchrotron Radiation Research Institute (JASRI) (Proposal No. 2006B1396). This research was supported by a Grants-in-Aid No. 18550191 from the Japan Society for the Promotion of Science. Also, this work was supported by "Innovation Creative Center for Advanced Interdisciplinary Research Areas (Shinshu university)" project in special coordination funds for promoting science and technology of the ministry of education, culture, sports, science and technology, the Japanese government.

References

[1] Br. Patent 578,097.
[2] Poulin-Dandurand S, Perez S, Revol JF, Brisse F. Polymer 1979;20:419.
[3] Deborough IJ, Hall IH, Neisser JZ. Polymer 1979;20:545.
[4] Wang B, Li CY, Hanzlicek J, Cheng SZD, Geil PH, Grebowicz J, et al. 2001;42:7171.
[5] Yang J, Sidoti G, Liu J, Geil PH, Li CY, Cheng SZD. Polymer 2001;42:7181.
[6] Grebowicz JS, Brown H, Chuah HH, Olvera JM, Wasiak A, Sajkiewicz P, et al. Polymer 2001;42:7153.
[7] Pyda M, Boller A, Grebowicz J, Chuah HH, Lebedev BV, Wunderlich B. J Polym Sci Part B Polym Phys 1998;36:2499.
[8] Wu J, Schultz JM, Samon JM, Pangelinan AB, Chuah HH. Polymer 2001;42:7161.
[9] Katayama K, Amano T, Nakamura K. Kolloid Z Z Polym 1968;226:125.
[10] Spruiell J, White J. Polym Eng Sci 1975;15:660.
[11] Haberkorn H, Hahn K, Breuer K. J Appl Polym Sci 1993;47:1551.
[12] Hsiao BS, Kennedy AD, Leach RA, Cho B, Harney P. J Appl Crystallogr 1997;30:1084.
[13] Yamaguchi T, Komoriyama K, Ohkoshi Y, Urakawa H, Gotoh Y, Terasawa N, et al. J Polym Sci Part B Polym Phys 2005;43:1090–9.
[14] Yamaguchi T, Kim KH, Murata T, Koide M, Hitoosa S, Urakawa H, et al. J Polym Sci Part B Polym Phys 2008;46:2126–42.
[15] Okumura W, Kanegae T, Ohkoshi Y, Gotoh Y, Nagura M. Intern Polym Processing 2003;18:1.
[16] Okumura W, Yamaguchi T, Ohkoshi Y, Gotoh Y, Nagura M. Intern Polym Processing 2002;17:124.
[17] Yamaguchi T, Ohkoshi Y, Gotoh Y, Nagura M. Seikei-Kakou 2005;17:649.
[18] Strobl GR, Schneider M. J Polym Sci Part B Polym Phys 1980;18:1343.